ELECTRONIC SUPPLEMENTARY INFORMATION

Structure and thermal properties relationships in the thermomaterial di-n-butylammonium tetrafluoroborate for multipurpose cooling and cold-storage

Javier García-Ben[a,‡], Juan Manuel Bermúdez-García[a,‡], Richard J. C. Dixey[b], Ignacio Delgado-Ferreiro[a], Antonio Luis Llamas-Saiz[c], Jorge López-Beceiro[d], Ramón Artiaga[d], Alberto García-Fernández[e], Ute B. Cappel[e], Bruno Alonso[f], Socorro Castro-García[a], Anthony E. Phillips[b], Manuel Sánchez-Andújar[a*] and María Antonia Señarís-Rodríguez[a**]

[a] *University of A Coruna, QUIMOLMAT Group, Dpt. Chemistry, Faculty of Science and Centro Interdisciplinar de Química e Bioloxía (CICA), Zapateira, 15071 A Coruña, Spain.*

[b] *School of Physical and Chemical Sciences, Queen Mary University of London, London, E1 4NS UK.*

[c] *Research Infrastructures Area, X-ray Unit, University of Santiago de Compostela,15782 Santiago de Compostela, Spain.*

[d] *Universidade da Coruña, Campus Industrial de Ferrol, CITENI-Grupo Proterm, Campus de Esteiro, 15403 Ferrol, Spain.*

[e] *Division of Applied Physical Chemistry, Department of Chemistry, KTH Royal Institute of Technology, SE-100 44 Stockholm, Sweden.*

[f] *ICGM, CNRS, Université de Montpellier, ENSCM, 34095 Montpellier Cedex 5, France.*

[‡] *These authors have equally contributed to this work.*

E-mail: m.andujar@udc.es, m.señaris.rodriguez@udc.es

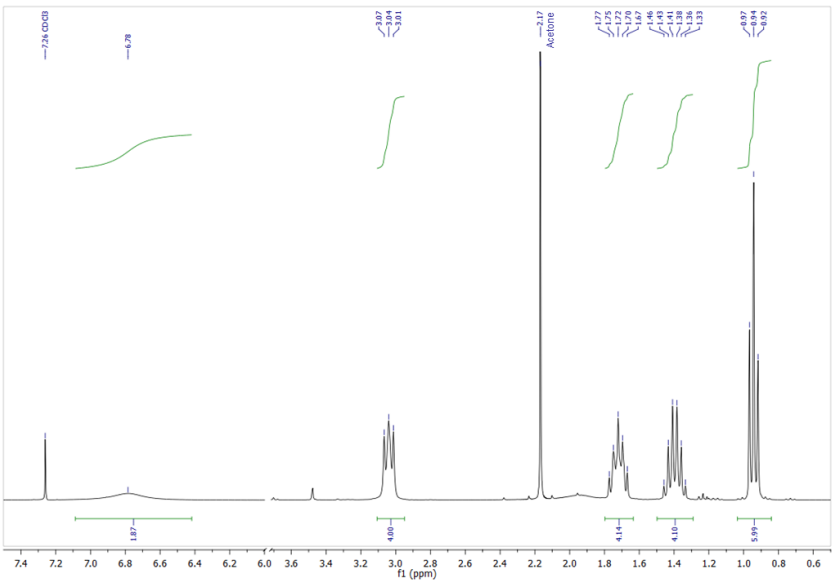

Fig. S1 Liquid ^{1}H-NMR of [DBA][BF_4] in $CDCl_3$.

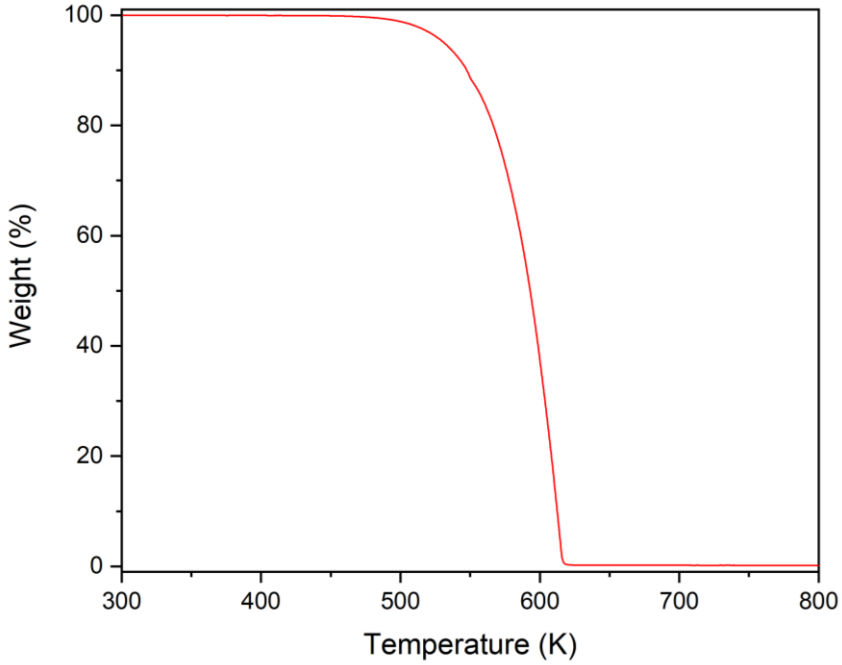

Fig. S2 Thermogravimetric analysis of [DBA][BF_4] under N_2 atmosphere.

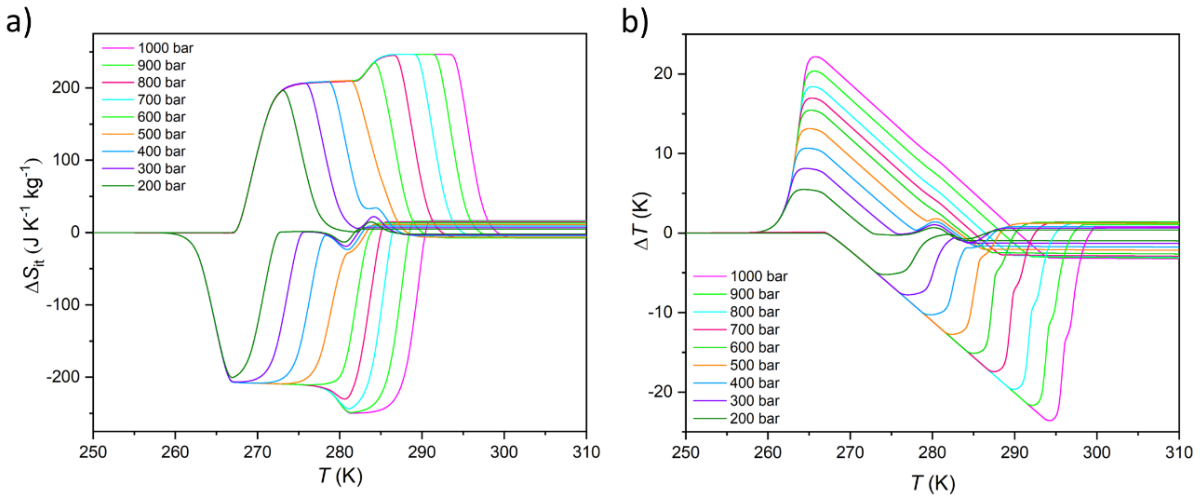

Fig. S3 a) Pressure-driven isothermal entropy changes on applying (0 → p) and removing (p → 0) pressure. b) Reversible adiabatic temperature changes on applying (0 → p) and removing (p → 0) pressure at different pressures.

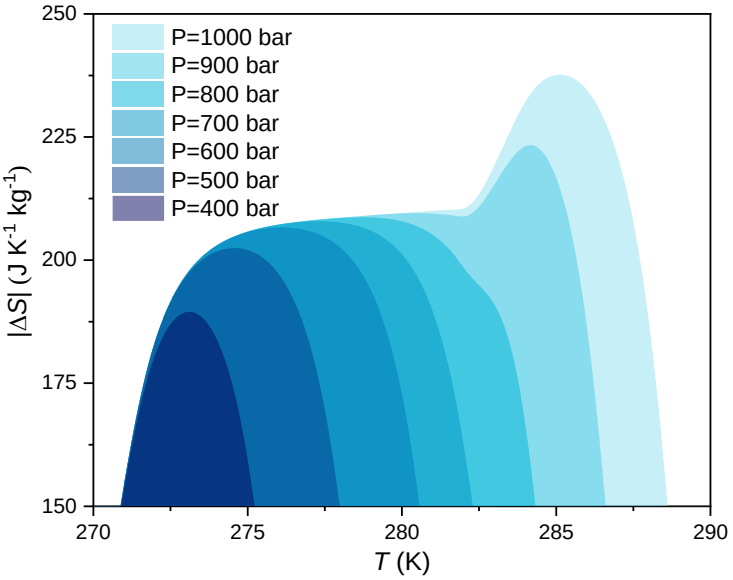

Fig. S4 Maximum reversible isothermal entropy changes of the (0 → p) curves at different pressures as a function of temperature.

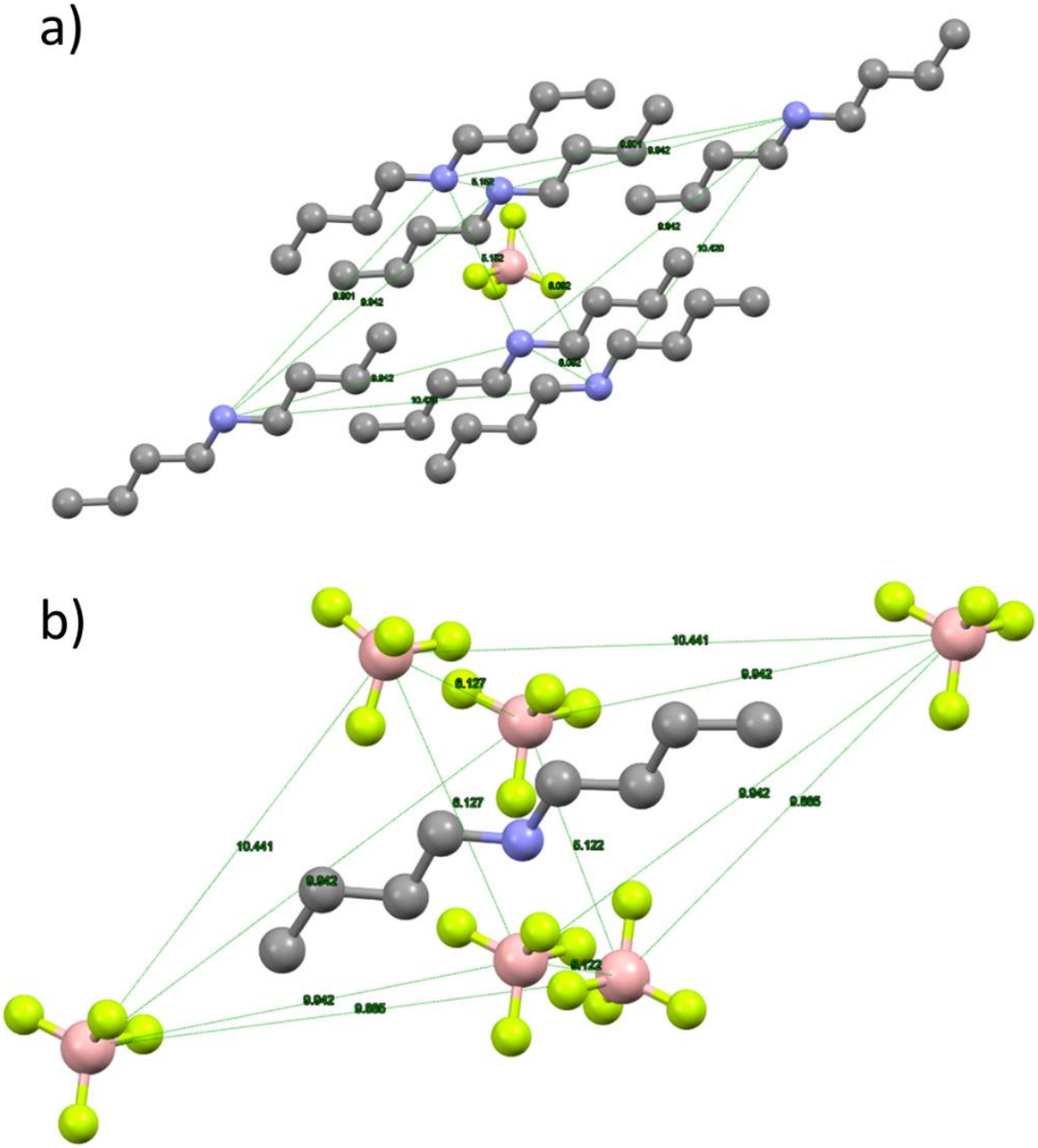

Fig. S5 Coordination environment of a) BF_4^- and b) DBA^+ in phase IV at T = 100 K.

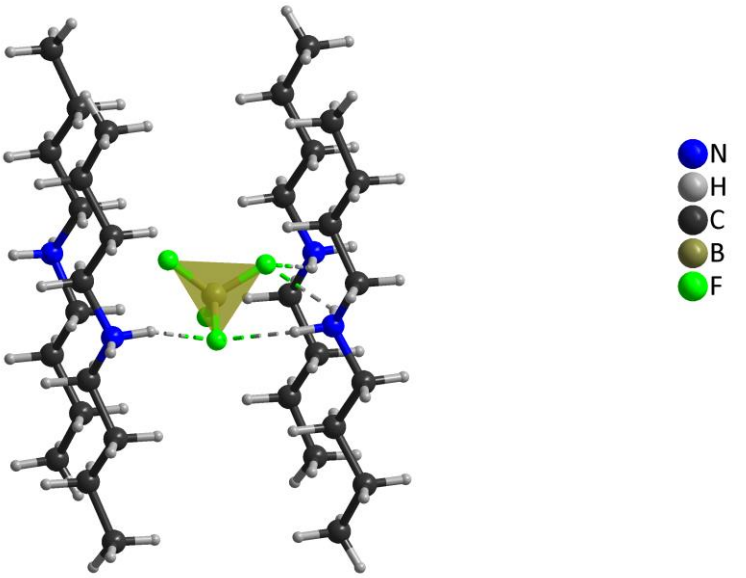

Fig. S6 H-Bonds of each $[BF_4]^-$ molecule in phase IV at T = 100 K.

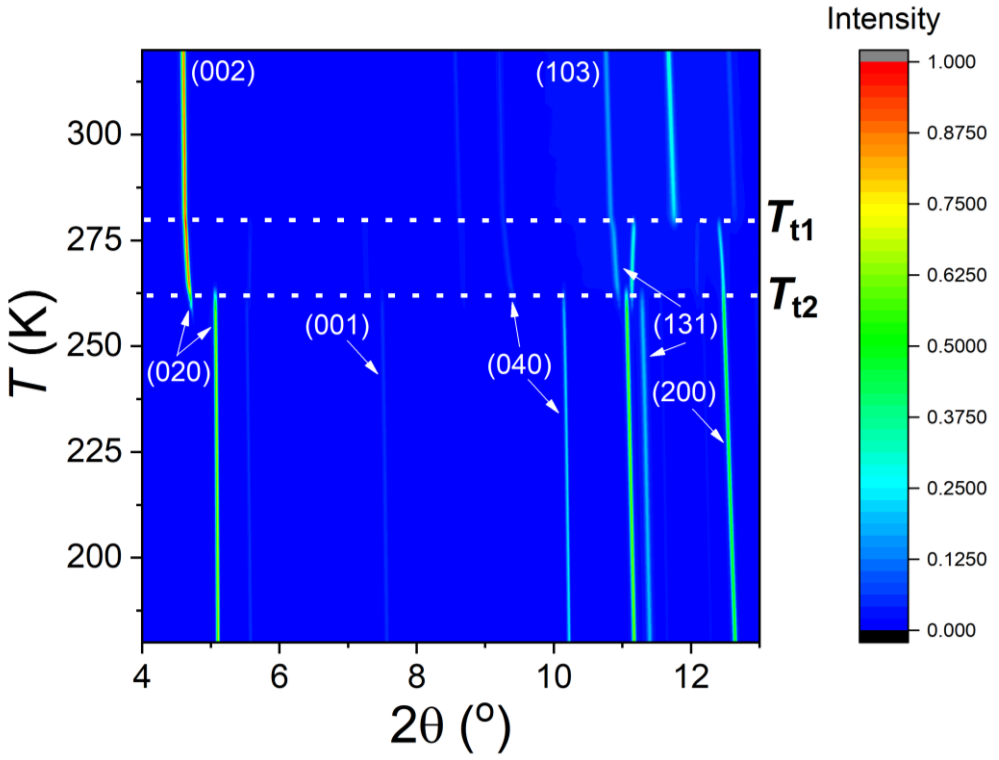

Fig. S7 SPXRD patterns of [DBA][BF_4] as a function of temperature (180 K < T < 320 K)].

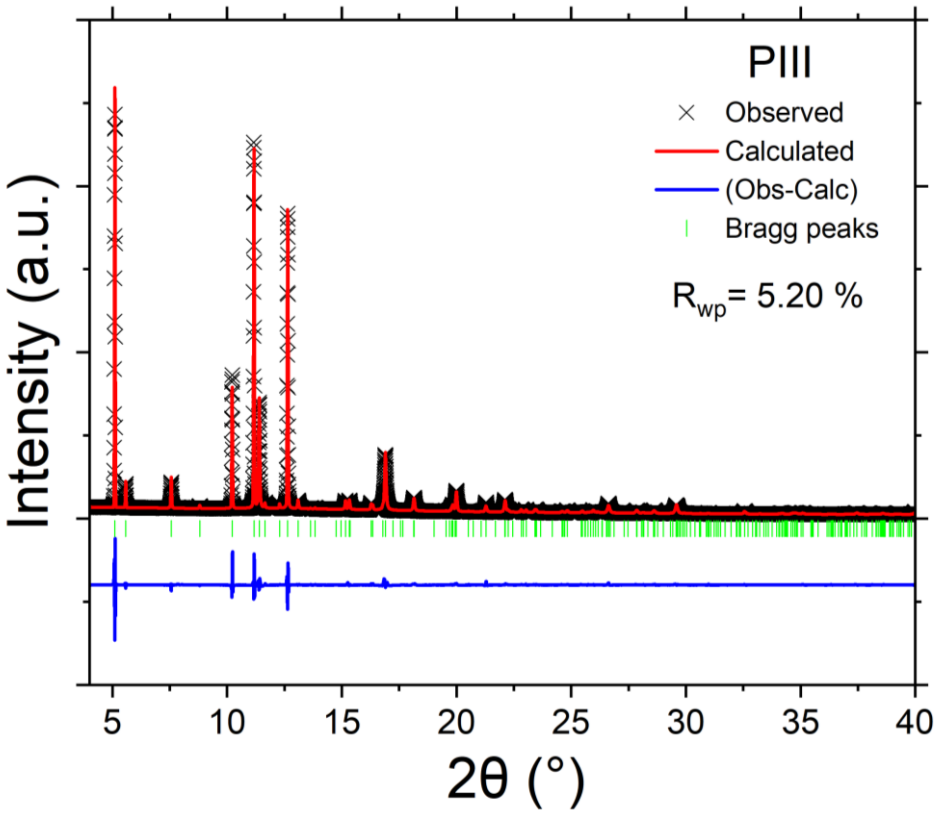

Fig. S8 Le Bail refinement of phase III of [DBA][BF_4] at T = 180 K.

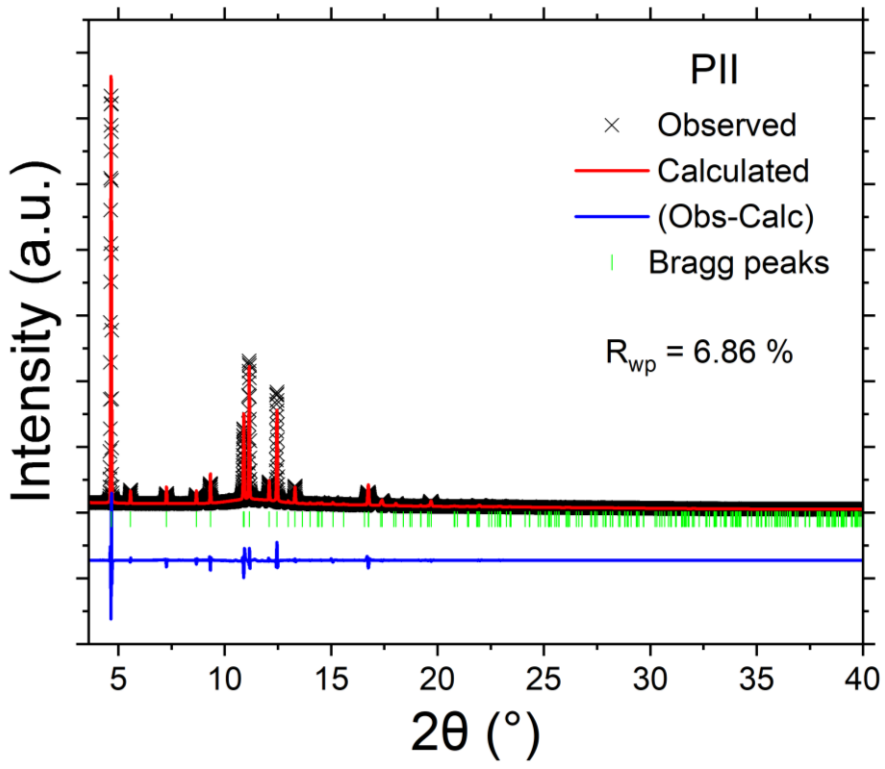

Fig. S9 Le Bail refinement of phase II of [DBA][BF_4] at T = 270 K.

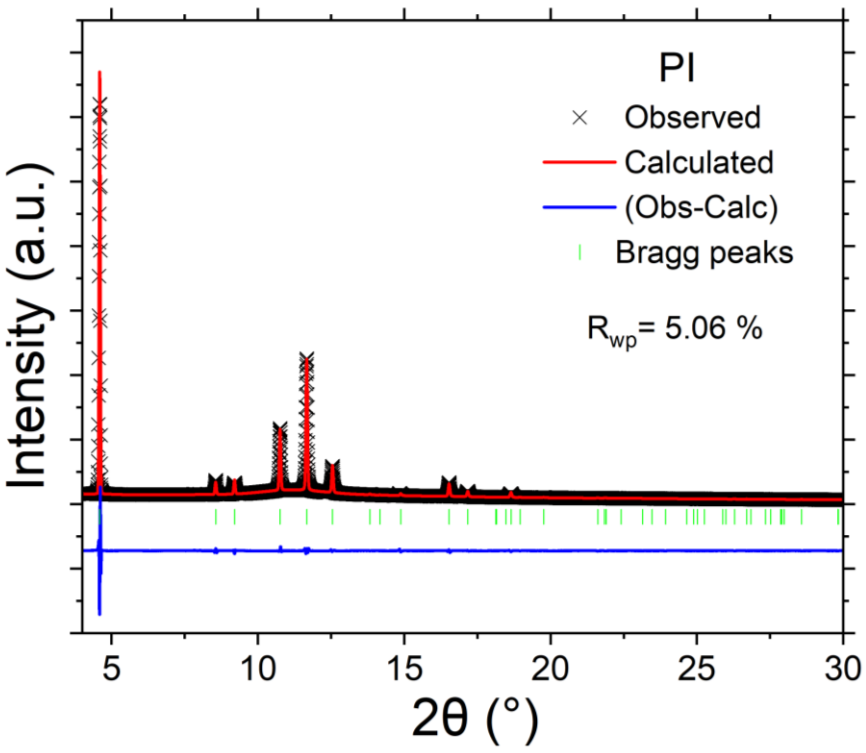

Fig. S10 Le Bail refinement of phase I of [DBA][BF_4] at T = 320 K.

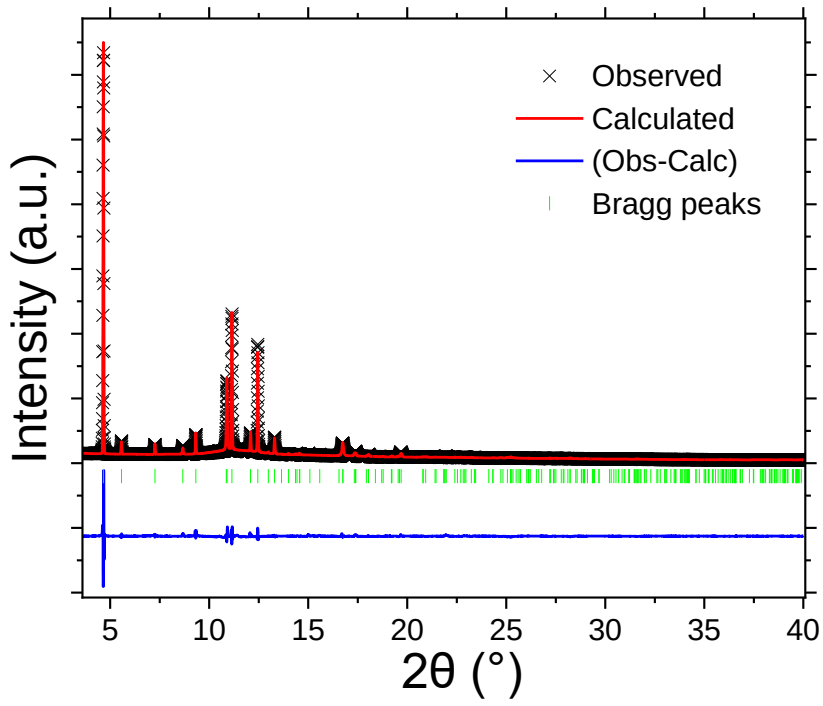

Fig. S11 Rietveld refinement of phase II of [DBA][BF_4] at T = 270 K

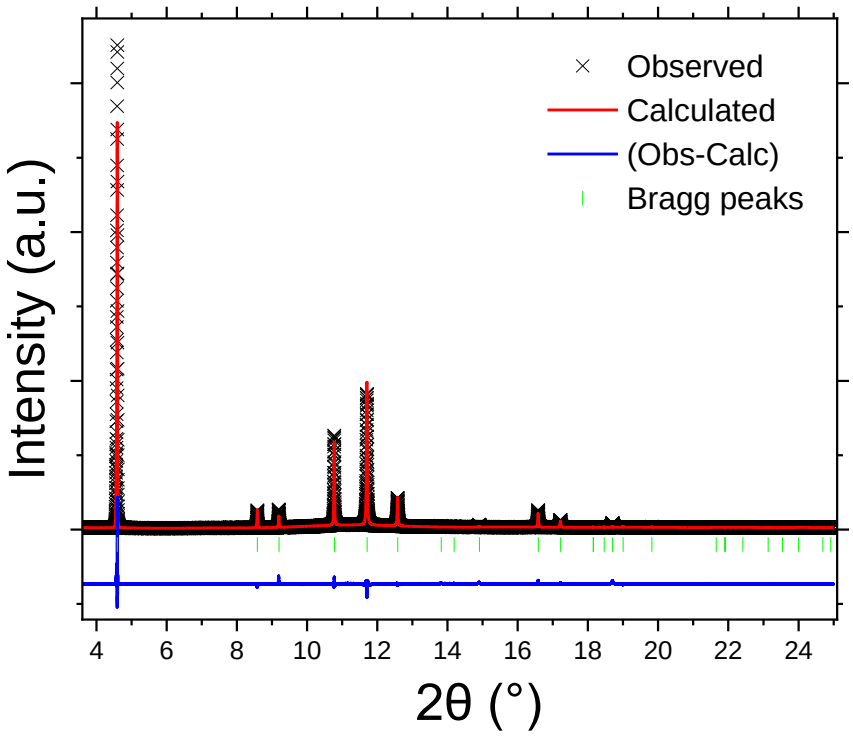

Fig. S12 Rietveld refinement of phase I of [DBA][BF_4] at T = 300 K.

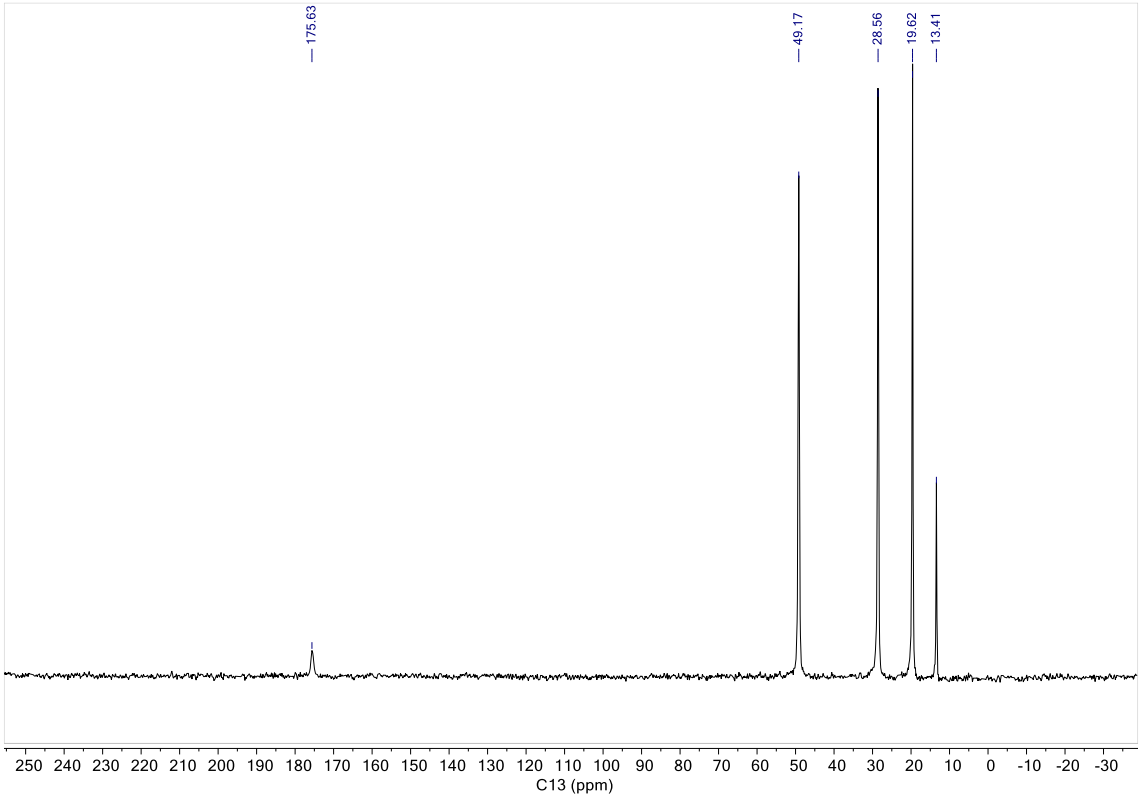

Fig. S13 $^{13}\{^{1}H\}$ CP-MAS spectra of phase I of [DBA][BF4] at T = 318 K.

Table S1. Data collection, cell and refinement parameters from the single crystal X-ray diffraction studies carried out at T = 100 K and T = 240 K for phases IV and III of [DBA][BF_4]

Empirical formula	**$C_8H_{20}N{\cdot}BF_4$**	**$C_8H_{20}N{\cdot}BF_4$**
Formula weight	217.06	217.06
Temperature	100.0(1) K	240.0(1) K
Wavelength	1.54178 Å	1.54178 Å
Crystal system	Orthorhombic	Orthorhombic
Space group	*Ccce*	*Cmme*
Unit cell dimensions	a = 7.3980(5) Å b = 18.4562(11) Å c = 16.8535(10) Å	a = 7.5762(10) Å b = 18.642(3) Å c = 8.5564(12) Å
Volume	2301.2(2) $Å^3$	1208.5(3) $Å^3$
Z	8	4
Density (calculated)	1.253 Mg/m^3	1.193 Mg/m^3
Absorption coefficient	1.02 mm^{-1}	0.97 mm^{-1}
F(000)	928	464
Crystal size	0.32 x 0.22x 0.08 mm^3	0.32 x 0.22x 0.08 mm^3
Theta range for data collection	5.3 to 67.8°	5.2 to 65.0°.
Index ranges	0<=h<=8 0<=k<=22 0<=l<=20	0<=h<=8 0<=k<=21 0<=l<=10
Reflections collected	50094	13977
Completeness (theta max.)	98.7 % (67.76º)	97.2 % (65.04º)
Refinement method	Full-matrix least-squares on F^2	Full-matrix least-squares on F^2
Data / restraints / parameters	1100 / 0 / 69	629 / 96 / 77
Goodness-of-fit on F^2	1.14	1.55
Final R indices [I>2sigma(I)]	R1 = 0.1091 wR2 = 0.3093	R1 = 0.1248 wR2 = 0.2748
R indices (all data)	R1 = 0.1310 wR2 = 0.3378	R1 = 0.1695 wR2 = 0.3096
Largest diff. peak and hole	0.61 and -0.32 $e.Å^{-3}$	0.48 and -0.28 $e.Å^{-3}$

Table S2. All the barocaloric materials represented in Fig. 5. *Note:* HOIM = Hybrid Organic-Inorganic Material, SP = Spin Crossover compound, OPC = Organic Plastic Crystal, POL = Polymer, AIS = Ammonium Inorganic Salt and MA = Metal Alloy. *Note2:* 24 and 25 are the same compound due to it has 2 phase transitions.

Number	Family	Material	REF	Number	Family	Material	REF
1	HOIM	$(C_{10}H_{21}NH_3)_2MnCl_4$	1	31	AIS	NH_4I	2
2	HOIM	$(C_9H_{19}NH_3)_2MnCl_4$	3	32	AIS	$(NH_4)_2MoO_2F_4$	4
3	HOIM	$(Me_3S)FeCl_4$	5	33	MA	$Ni_{50}Mn_{31.5}Ti_{18.5}$	6
4	HOIM	$(Me_3(ClMe)N)FeCl_4$	5	34	MA	$MnNiSi_{0.59}FeCoGe_{0.41}$	7
5	HOIM	$(C_9H_{19}NH_3)_2CuBr_4$	3	35	MA	$LaFe_{11.33}Co_{0.47}Si_{1.2}$	8
6	HOIM	$[Me_4N][Mn(N_3)_3]$	9	36	MA	Mn_3NiN	10
7	HOIM	$[Pr_4N][Mn(N(CN)_2)_3]$	11	37	MA	$Gd_2Si_5Ge_5$	12
8	HOIM	$[Pr_4N][Cd(N(CN)_2)_3]$	13	38	MA	$Ni_{0.95}Fe_{0.05}S$	14
9	HOIM	$[Me_2NH_2][Mg(HCOO)_3]$	15	39	MA	$Ni_{44.6}Co_{5.5}Mn_{35.5}In_{14.4}$	16
10	SC	$[FeL_2][BF_4]_2$	17	40	MA	$Ni_{2.00}Mn_{1.32}In_{0.68}$	18
11	SC	$[Fe(hyptrz)_3]A_2{\cdot}H_2O$	19	41	MA	$Co_{50}Fe_{2.5}V_{31.5}Ga_{16}$	20
12	SC	$Fe_3(bntrz)_6(tcnset)_6$	21	42	MA	$MnNiSi_{0.60}FeCoGe_{0.40}$	22
13	SC	$Fe[HB(tz)_3]_2$	23	43	MA	$MnCoGeB_{0.03}$	24
14	OPC	$(CH_3)C(CH_2OH)_3$	25	44	MA	Mn_3GaN	26
15	OPC	$(CH_3)_2C(CH_2OH)_2$	27	45	MA	$Ni_{35.5}Co_{14.5}Mn_{35}Ti_{15}$	28
16	OPC	$C_{11}H_{18}O$	29	46	MA	$Ni_{49.26}Mn_{36.08}In_{14.66}$	7
17	OPC	$(CH_3)_3C(CH_2OH)$	25	47	MA	$Ni_{0.875}Fe_{0.125}S$	14
18	OPC	$C_{10}H_{15}Cl$	30	48	MA	$Ni_{0.85}Fe_{0.15}S$	14
19	OPC	o-$C_2B_7H_{12}$	31	49	MA	$Ni_{1.99}Mn_{1.34}In_{0.67}$	18
20	OPC	m-$C_2B_7H_{12}$	31	50	MA	$Fe_{49}Rh_{51}$	32
21	OPC	p-$C_2B_7H_{12}$	31	51	MA	$MnCoGe_{0.99}In_{0.01}$	33
22	OPC	$C_{10}H_{15}Br$	30	52	MA	$MnNiSi_{0.61}FeCoGe_{0.39}$	22
23	OPC	1- $C_{10}H_{15}O$	29	53	MA	$Ni_{0.825}Fe_{0.175}S$	14
24	OPC	2- $C_{10}H_{15}O$	29	54	MA	$Ni_{58.3}Mn_{17.1}Ga_{24.6}$	34
25	OPC	2- $C_{10}H_{15}O$	29	55	MA	$Ni_{42.3}Co_{7.9}Mn_{38.8}Sn_{11.0}$	35
26	OPC	C_{60}	36	56	MA	$Ni_{1.99}Mn_{1.37}In_{0.64}$	18
27	POL	Acetoxy Silicone Rubber	37	57	MA	$Ni_{2.05}Mn_{1.30}In_{0.65}$	18
28	POL	PVDF-TrFE-CTFE	38	58	MA	$MnNiSi_{0.62}FeCoGe_{0.38}$	22
29	AIS	NH_4HSO_4	39	59	MA	$Ni_{2.02}Mn_{1.36}In_{0.62}$	18
30	AIS	$(NH_4)_2NbOF_5$	40				

Table S3. Atom distances and Rietveld refinement parameters of phase II.

Unit cell: *a* = 7.62273, *b* = 20.34391, *c* = 8.51112

Final refinement: *wR* = 5.92% on 9126 observations in this histogram

Other residuals: *R* = 3.45%, *R-bkg* = 8.29%, *wR-bkg* = 5.92% *wRmin* = 0.41%

Atom name	**x**	**y**	**z**	**Occ.**	**Uiso**
N1	0	0.75	0.27243	1	0.11078
C2	0	0.68191	0.20262	1	0.10748
C3	0	0.64166	0.29171	1	0.11633
C4	0	0.58008	0.18323	1	0.1233
C5	0.08897	0.51155	0.29982	0.5	0.23804
B1_1	0.495	0.7494	0.2854	0.25	0.17123
F1_1	0.49964	0.68345	0.16725	0.25	0.17313
F2_1	0.33725	0.78389	0.32159	0.25	0.30528
F3_1	0.57343	0.71161	0.42633	0.25	0.34777
F4_1	0.5873	0.79578	0.24478	0.25	0.1503

Table S4. Atom distances and Rietveld refinement parameters of phase I.

Unit Cell: *a* = 5.73161, *b* = 5.73161, *c* = 20.61450

Final refinement: *wR* = 8.98% on 21501 observations in this histogram

Other residuals: *R* = 6.70%, *R-bkg* = 8.25%, *wR-bkg* = 8.98% *wRmin* = 3.48%

Atom name	**x**	**y**	**z**	**Occ.**	**Uiso**
B	0	0	0.47	0.5	0.30668
F1	0	0	0.41	0.5	0.31835
F2	0.18501	0	0.5	0.25	0.39494
N4	0	0	0	1	0.92652
C1	0.95817	0.04183	0.0851	0.125	0.58818
C2	0.95552	0.04448	0.12233	0.125	0.30176
C3	0.91324	0.08676	0.19077	0.125	0.4033
C4	0.82974	0.17026	0.22989	0.125	0.40361

References

1 J. Li, M. Barrio, D. J. Dunstan, R. Dixey, X. Lou, J. L. Tamarit, A. E. Phillips and P. Lloveras, *Adv. Funct. Mater.*, 2021, **31**, 1–8.

2 Q. Ren, J. Qi, D. Yu, Z. Zhang, R. Song, W. Song, B. Yuan, T. Wang, W. Ren, Z. Zhang, X. Tong and B. Li, *Nat. Commun.*, 2022, **13**, 1–9.

3 Y. Gao, H. Liu, F. Hu, H. Song, H. Zhang, J. Hao, X. Liu, Z. Yu, F. Shen, Y. Wang, H. Zhou, B. Wang, Z. Tian, Y. Lin, C. Zhang, Z. Yin, J. Wang, Y. Chen, Y. Li, Y. Song, Y. Shi, T. Zhao, J. Sun, Q. Huang and B. Shen, *NPG Asia Mater.*, , DOI:10.1038/s41427-022-00378-4.

4 M. V. Gorev, E. V. Bogdanov, I. N. Flerov, A. G. Kocharova and N. M. Laptash, *Phys. Solid State*, 2010, **52**, 167–175.

5 J. Salgado-Beceiro, J. M. Bermúdez-García, E. Stern-Taulats, J. García-Ben, S. Castro-García, M. Sánchez-Andújar, X. Moya and M. A. Señarís-Rodríguez, *ChemRxiv*, 2021, 17–19.

6 A. Aznar, A. Gràcia-Condal, A. Planes, P. Lloveras, M. Barrio, J. L. Tamarit, W. Xiong, D. Cong, C. Popescu and L. Mañosa, *Phys. Rev. Mater.*, 2019, **3**, 1–7.

7 L. Mañosa, D. González-Alonso, A. Planes, E. Bonnot, M. Barrio, J. L. Tamarit, S. Aksoy and M. Acet, *Nat. Mater.*, 2010, **9**, 478–481.

8 L. Mañosa, D. González-Alonso, A. Planes, M. Barrio, J. L. Tamarit, I. S. Titov, M. Acet, A. Bhattacharyya and S. Majumdar, *Nat. Commun.*, 2011, **2**, 1–5.

9 J. Salgado-Beceiro, A. Nonato, R. X. Silva, A. García-Fernández, M. Sánchez-Andújar, S. Castro-García, E. Stern-Taulats, M. A. Señarís-Rodríguez, X. Moya and J. M. Bermúdez-García, *Mater. Adv.*, 2020, **1**, 3167–3170.

10 D. Boldrin, E. Mendive-Tapia, J. Zemen, J. B. Staunton, T. Hansen, A. Aznar, J. L. Tamarit, M. Barrio, P. Lloveras, J. Kim, X. Moya and L. F. Cohen, *Phys. Rev. X*, 2018, **8**, 41035.

11 J. M. Bermúdez-García, M. Sánchez-Andújar, S. Castro-García, J. López-Beceiro, R. Artiaga and M. A. Señarís-Rodríguez, *Nat. Commun.*, , DOI:10.1038/ncomms15715.

12 S. Yuce, M. Barrio, B. Emre, E. Stern-Taulats, A. Planes, J. L. Tamarit, Y. Mudryk, K. A. Gschneidner, V. K. Pecharsky and L. Mañosa, *Appl. Phys. Lett.*, , DOI:10.1063/1.4745920.

13 J. M. Bermúdez-García, S. Yáñez-Vilar, A. García-Fernández, M. Sánchez-Andújar, S. Castro-García, J. López-Beceiro, R. Artiaga, M. Dilshad, X. Moya and M. A. Señarís-Rodríguez, *J. Mater. Chem. C*, 2018, **6**, 9867–9874.

14 J. Lin, P. Tong, X. Zhang, Z. Wang, Z. Zhang, B. Li, G. Zhong, J. Chen, Y. Wu, H. Lu, L. He, B. Bai, L. Ling, W. Song, Z. Zhang and Y. Sun, *Mater. Horizons*, 2020, **7**, 2690–2695.

15 M. Szafrański, W. J. Wei, Z. M. Wang, W. Li and A. Katrusiak, *APL Mater.*, , DOI:10.1063/1.5049116.

16 X. He, S. Wei, Y. Kang, Y. Zhang, Y. Cao, K. Xu, Z. Li and C. Jing, *Scr. Mater.*, 2018, **145**, 58–61.

17 S. P. Vallone, A. N. Tantillo, A. M. dos Santos, J. J. Molaison, R. Kulmaczewski, A. Chapoy, P. Ahmadi, M. A. Halcrow and K. G. Sandeman, *Adv. Mater.*, 2019, **31**, 1–7.

18 E. Stern-Taulats, A. Planes, P. Lloveras, M. Barrio, J. L. Tamarit, S. Pramanick, S. Majumdar, S. Yüce, B. Emre, C. Frontera and L. Mañosa, *Acta Mater.*, 2015, **96**, 324–332.

19 P. J. Von Ranke, B. P. Alho, R. M. Ribas, E. P. Nobrega, A. Caldas, V. S. R. De Sousa, M. V. Colaço, L. F. Marques, D. L. Rocco and P. O. Ribeiro, *Phys. Rev. B*, 2018, **98**, 2–6.

20 H. Liu, Z. Li, Y. Zhang, Z. Ni, K. Xu and Y. Liu, *Scr. Mater.*, 2020, **177**, 1–5.

21 M. Romanini, Y. Wang, G. Kübra, G. Ornelas, P. Lloveras, Y. Zhang, W. Zheng, M. Barrio, A. Aznar, A. Gràcia-Condal, B. Emre, O. Atakol, C. Popescu, H. Zhang, Y. Long, L. Balicas, J. L. Tamarit, A. Planes, M. Shatruk and L. Mañosa, *Adv. Mater.*, 2021, **33**, 2008076.

22 P. Lloveras, T. Samanta, M. Barrio, I. Dubenko, N. Ali, J. L. Tamarit and S. Stadler, *APL Mater.*, 2019, **7**, 0–9.

23 J. Seo, J. D. Braun, V. M. Dev and J. A. Mason, *J. Am. Chem. Soc.*, 2022, **144**, 6493–6503.

24 A. Aznar, P. Lloveras, J. Y. Kim, E. Stern-Taulats, M. Barrio, J. L. Tamarit, C. F. Sánchez-Valdés, J. L. Sánchez Llamazares, N. D. Mathur and X. Moya, *Adv. Mater.*, 2019, **31**, 1–6.

25 A. Aznar, P. Lloveras, M. M. Barrio, P. Negrier, A. Planes, L. L. Mañosa, N. D. Mathur, X. Moya and J. L. L. Tamarit, *J. Mater. Chem. A*, 2020, **8**, 639–647.

26 D. Matsunami, A. Fujita, K. Takenaka and M. Kano, *Nat. Mater.*, 2015, **14**, 73–78.

27 P. Lloveras, A. Aznar, M. Barrio, P. Negrier, C. Popescu, A. Planes, L. Mañosa, E. Stern-Taulats, A. Avramenko, N. D. Mathur, X. Moya and J. L. Tamarit, *Nat. Commun.*, 2019, **10**, 1–7.

28 Z. Wei, Y. Shen, Z. Zhang, J. Guo, B. Li, E. Liu, Z. Zhang and J. Liu, *APL Mater.*, ,

DOI:10.1063/5.0005021.

29 A. Salvatori, P. Negrier, A. Aznar, M. Barrio, J. L. Tamarit and P. Lloveras, , DOI:10.1063/5.0127667.

30 A. Aznar, P. Negrier, A. Planes, L. Mañosa, E. Stern-Taulats, X. Moya, M. Barrio, J. L. Tamarit and P. Lloveras, *Appl. Mater. Today*, 2021, **23**, 101023.

31 K. Zhang, R. Song, J. Qi, Z. Zhang, Z. Zhang, C. Yu, K. Li, Z. Zhang and B. Li, *Adv. Funct. Mater.*, , DOI:10.1002/adfm.202112622.

32 E. Stern-Taulats, A. Planes, P. Lloveras, M. Barrio, J. L. Tamarit, S. Pramanick, S. Majumdar, C. Frontera and L. Mañosa, *Phys. Rev. B - Condens. Matter Mater. Phys.*, 2014, **89**, 1–8.

33 R. R. Wu, L. F. Bao, F. X. Hu, H. Wu, Q. Z. Huang, J. Wang, X. L. Dong, G. N. Li, J. R. Sun, F. R. Shen, T. Y. Zhao, X. Q. Zheng, L. C. Wang, Y. Liu, W. L. Zuo, Y. Y. Zhao, M. Zhang, X. C. Wang, C. Q. Jin, G. H. Rao, X. F. Han and B. G. Shen, *Sci. Rep.*, 2015, **5**, 1–11.

34 X. J. He, K. Xu, S. X. Wei, Y. L. Zhang, Z. Li and C. Jing, *J. Mater. Sci.*, 2017, **52**, 2915–2923.

35 X. He, Y. Kang, S. Wei, Y. Zhang, Y. Cao, K. Xu, Z. Li, C. Jing and Z. Li, *J. Alloys Compd.*, 2018, **741**, 821–825.

36 J. Li, D. Dunstan, X. Lou, A. Planes, L. Mañosa, M. Barrio, J. L. Tamarit and P. Lloveras, *J. Mater. Chem. A*, 2020, **8**, 20354–20362.

37 W. Imamura, É. O. Usuda, L. S. Paixão, N. M. Bom, A. M. Gomes and A. M. G. Carvalho, *Chinese J. Polym. Sci. (English Ed.*, 2020, **38**, 999–1005.

38 E. O. Usuda, N. M. Bom and A. M. G. Carvalho, *Eur. Polym. J.*, 2017, **92**, 287–293.

39 P. J. von Ranke, B. P. Alho and P. O. Ribeiro, *J. Alloys Compd.*, 2018, **749**, 556–560.

40 M. V. Gorev, E. V. Bogdanov, I. N. Flerov, V. N. Voronov and N. M. Laptash, *Ferroelectrics*, 2010, **397**, 76–80.